

See discussions, stats, and author profiles for this publication at: <https://www.researchgate.net/publication/280628605>

Conformational Heterogeneity Determined by Folding and Oligomer Assembly Routes of the Interferon Response Inhibitor NS1 Protein, Unique to Human Respiratory Syncytial Virus

ARTICLE *in* BIOCHEMISTRY · AUGUST 2015

Impact Factor: 3.02 · DOI: 10.1021/acs.biochem.5b00615 · Source: PubMed

READS

77

5 AUTHORS, INCLUDING:



Esteban Pretel

Biosidus

8 PUBLICATIONS 14 CITATIONS

[SEE PROFILE](#)



Ignacio Enrique Sánchez

University of Buenos Aires

44 PUBLICATIONS 984 CITATIONS

[SEE PROFILE](#)



Lucia B Chemes

Fundación Instituto Leloir

18 PUBLICATIONS 208 CITATIONS

[SEE PROFILE](#)



Gonzalo de Prat-Gay

Fundación Instituto Leloir

96 PUBLICATIONS 1,822 CITATIONS

[SEE PROFILE](#)

Conformational Heterogeneity Determined by Folding and Oligomer Assembly Routes of the Interferon Response Inhibitor NS1 Protein, Unique to Human Respiratory Syncytial Virus

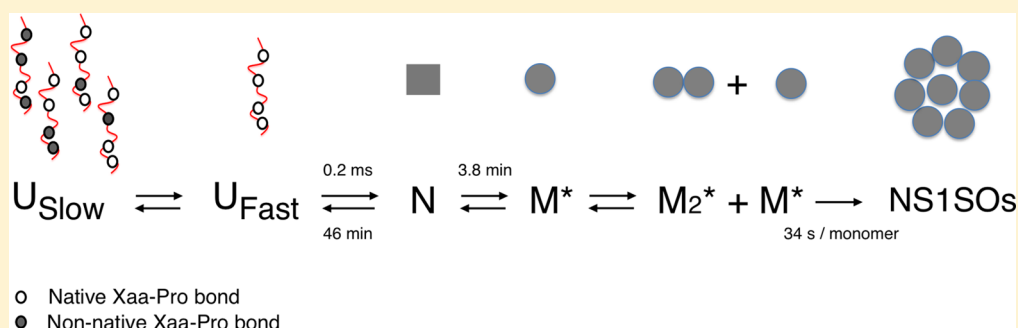
Esteban Pretel,[†] Ignacio E. Sánchez,[‡] Marisol Fassolari,[†] Lucía B. Chemes,[†] and Gonzalo de Prat-Gay^{*,†,§}

[†]Protein Structure-Function and Engineering Laboratory, Fundación Instituto Leloir and IIBBA-CONICET, Av. Patricias Argentinas 435, 1405 Buenos Aires, Argentina

[‡]Protein Physiology Laboratory, Departamento de Química Biológica, Facultad de Ciencias Exactas y Naturales and IQUIBICEN-CONICET, Universidad de Buenos Aires, Buenos Aires, Argentina

[§]Ciência Sem Fronteiras Senior Fellow, CNPq, Laboratório de Genômica Estrutural, Instituto de Biofísica Carlos Chagas Filho, Universidade Federal do Rio de Janeiro, Rio de Janeiro, RJ, Brazil

Supporting Information



ABSTRACT: The nonstructural NS1 protein is an essential virulence factor of the human respiratory syncytial virus, with a predominant role in the inhibition of the host antiviral innate immune response. This inhibition is mediated by multiple protein–protein interactions and involves the formation of large oligomeric complexes. There is neither a structure nor sequence or functional homologues of this protein, which points to a distinctive mechanism for blocking the interferon response among viruses. The NS1 native monomer follows a simple unfolding kinetics via a nativelylike transition state ensemble, with a half-life of 45 min, in agreement with a highly stable core structure at equilibrium. Refolding is a complex process that involves several slowly interconverting species compatible with proline isomerization. However, an ultrafast folding event with a half-life of 0.2 ms is indicative of a highly folding compatible species within the unfolded state ensemble. On the other hand, the oligomeric assembly route from the native monomer, which does not involve unfolding, shows a monodisperse and irreversible end-point species triggered by a mild temperature change, with half-lives of 160 and 26 min at 37 and 47 °C, respectively, and at a low protein concentration (10 μM). A large secondary structure change into β-sheet structure and the formation of a dimeric nucleus precede polymerization by the sequential addition of monomers at the surprisingly low rate of one monomer every 34 s. The polymerization phase is followed by the binding to thioflavin-T indicative of amyloid-like, albeit soluble, repetitive β-sheet quaternary structure. The overall process is reversible only up until ~8 min, a time window in which most of the secondary structure change takes place. NS1's multiple binding activities must be accommodated in a few binding interfaces at most, something to be considered remarkable given its small size (15 kDa). Thus, conformational heterogeneity, and in particular oligomer formation, may provide a means of expand its binding repertoire. These equilibria will be determined by variables such as macromolecular crowding, protein–protein interactions, expression levels, turnover, or specific subcellular localization. The irreversible and quasi-spontaneous nature of the oligomer assembly, together with the fact that NS1 is the most abundant viral protein in infected cells, makes its accumulation highly conceivable under conditions compatible with the cellular milieu. The implications of NS1 oligomers in the viral life cycle and the inhibition of host innate immune response remain to be determined.

Paramyxoviruses make up a diverse family of enveloped nonsegmented negative-strand RNA viruses that belong to the order of Mononegavirales. Some of them are the most ubiquitous disease-causing viruses of humans and animals, including human parainfluenza viruses type 1–4, mumps, measles, and other lethal zoonotic viruses such as Nipah and

Hendra from the Paramyxovirinae subfamily. Human respiratory syncytial virus (hRSV), a member of the Pneumovirinae

Received: June 4, 2015

Revised: July 30, 2015



41 subfamily,¹ is the leading cause of lower respiratory tract disease
42 among young children and immunocompromised individuals.
43 hRSV infection is one of the most frequent reasons for
44 hospitalization in developing countries, where 99% of hRSV-
45 related deaths take place.² In addition, hRSV infection is
46 believed to be associated with long-term complications, such as
47 recurrent wheezing and asthma.³ Despite the fact that during
48 the last decades there has been significant progress in the
49 understanding of hRSV pathogenesis, there is no antiviral
50 treatment or effective vaccine available at present.^{4,5}

51 Paramyxoviruses induce a wide variety of host responses
52 upon infection. The first line of host defense against infection is
53 the activation of the interferon (IFN) pathways. The IFN
54 induction pathway is initiated by the activation of the RIG-I
55 cytoplasmic RNA sensor, which recognizes viral RNA
56 products.⁶ Through its CARD domain, RIG-I activates the
57 signaling adaptor MAVS,⁷ located in the outer membrane of
58 mitochondria. MAVS activation by RIG-I leads to polymer-
59 ization of inactive MAVS monomers into functional amyloid-
60 like oligomers docked on the surface of the mitochondrial
61 membrane,⁸ which amplifies signaling of the IFN induction
62 pathway and activates transcription of IFN-regulated genes.
63 Produced IFN is secreted and is able to interact with IFN
64 receptors, thus triggering the IFN response pathway. This
65 signaling pathway promotes the phosphorylation and activation
66 of signal transducer and activation of transcription proteins
67 (STAT 1 and 2), which translocate to the nucleus and lead to
68 transcriptional activation of responsive genes encoding proteins
69 with antiviral effects.^{9,10}

70 To evade these antiviral defense mechanisms, Paramyxo-
71 viruses evolved different strategies, which result in a decreased
72 level of IFN production or disruption of the IFN signaling
73 pathways, leading to enhanced disease. Inhibition of IFN
74 synthesis by Paramyxoviruses includes mechanisms such as the
75 inhibition of cellular RNA sensors, control of aberrant viral
76 RNA synthesis, signaling kinases, and suppression of the IFN
77 promoter. The mechanisms related to inhibition of IFN
78 signaling include sequestration of signaling factors, upregulation
79 of cellular inhibitory molecules, and targeted degradation of
80 signaling products.¹¹ This inhibition of IFN signaling is
81 mediated by RSV nonstructural (NS) proteins NS1 and NS2,
82 which are unique to RSV and show no sequence homology to
83 other known viral or cellular proteins, even within the
84 Paramyxoviruses.¹² The NS proteins have been shown to
85 target different members of the interferon (IFN) induction and
86 response pathways, decreasing levels of IFN α and β .^{13–22} NS2
87 was shown to interact with RIG-I, inhibiting RIG-I–MAVS
88 binding and downstream signal transduction.²³ Furthermore, in
89 another report, the interaction between MAVS and NS1 was
90 investigated, and it was found that this binding interferes with
91 the RIG-I–MAVS interaction, and that recombinant viruses
92 lacking NS1 do not seem to affect this interaction.^{15,19,24} It was
93 shown that NS proteins, predominantly NS2, decrease levels of
94 STAT2, promoting its proteasomal degradation.^{12,16,25} In
95 addition, NS1 and NS2 may play a role in RNA replication,
96 with a stronger inhibitory effect reported for NS1 than for
97 NS2.²⁶

98 Given the relevance of NS1 and its uniqueness to RSV
99 among all Paramyxoviruses, the lack of information about the
100 structure and biochemical activity that underlies its biological
101 function is noticeable. Previously, we and others showed that
102 the 15.5 kDa NS1 protein is a stable monomer in solution.^{27,28}
103 Chemical denaturation experiments showed that the NS1

monomer unfolds following a highly cooperative two-state and
fully reversible reaction.²⁸ However, under mild conditions
compatible with the intracellular environment, conformational
changes are induced, leading to the formation of large (~150
monomer units) soluble spherical oligomers (NS1SOs) as
determined by atomic force microscopy and dynamic light
scattering assays.²⁸ These oligomers are highly stable and
homogeneous species with similar size and shape in solution
and present repetitive β -sheet structures that bind Congo red
and thioflavin T dyes. Recent functional data suggest that NS1
oligomerization may be relevant *in vivo*. Namely, NS1
transfected in lung epithelial cells was shown to form homo-
oligomers and to interact with NS2.²⁰ Moreover, a large
heterogeneous protein complex called the “degradosome” has
been described, which has a molecular mass in the range of
300–750 kDa and contains both NS1 and NS2 proteins as well
as proteasome subunits. The degradosome presents degradative
activity for many NS1 and NS2 cellular targets, such as RIG-I,
TRAF3, and STAT2, and was found to be important in innate
immunity suppression in infected cells.²⁹ These findings could
indicate that the NS1SOs formed quasi-spontaneously *in vitro*
could be correlated to the “degradosome” complex and may
represent a functionally relevant species *in vivo*.

In this work, with the goal of understanding the binding
promiscuity of this unique protein, we set out to investigate the
folding mechanism of the monomer and the assembly
mechanism of the NS1 oligomer. Using different spectroscopic
techniques, we found folding kinetics to be a complex process,
in contrast to the simple two-state behavior shown at
equilibrium and in unfolding kinetics. We dissected the
oligomerization mechanism and propose a model of NS1 self-
assembly. After an initial step involving a reversible nucleation
intermediate, the reaction proceeds irreversibly, leading to the
formation of spherical particles. We discuss the results in
connection with its known and hypothesized activities related
to its capacity to inhibit the interferon response.

EXPERIMENTAL PROCEDURES

Expression and Purification of the hRSV NS1 Protein.

The human RSV strain A NS1 protein was recombinantly
expressed and purified as previously described.²⁸ Briefly,
C41(DE3) cells harboring plasmid pMal 2C, with the NS1
sequence cloned as a thrombin cleavage fusion protein to the
maltose binding protein (MBP), were grown in LB medium at
an OD of 0.6, and protein expression was induced with 0.3 mM
isopropyl β -D-1-thiogalactopyranoside, after which cells were
incubated at 20 °C for 16 h. The soluble protein was
precipitated with 50% ammonium sulfate, resuspended, and
purified with an affinity amylose resin (New England Biolabs,
Hitchin, U.K.), followed by a thrombin treatment and size
exclusion chromatography to cleave and separate NS1 from the
fusion protein MBP. Pure NS1 was dialyzed against 10 mM
Tris-HCl buffer (pH 8.0), 0.2 M NaCl, and 1 mM DTT. The
protein concentration was determined spectrophotometrically
using a molar extinction coefficient (ϵ_{280}) of 9970 M⁻¹ cm⁻¹.

Circular Dichroism and Fluorescence Spectroscopy.

Far-UV circular dichroism (CD) measurements were per-
formed on a Jasco J-810 spectropolarimeter using a Peltier
temperature-controlled sample holder at 20 °C. Spectra were
recorded between 200 and 260 nm at a scan rate of 100 nm/
min, with a response time of 4 s and a bandwidth of 2 nm. All
spectra were an average of at least four to six scans. Raw data

165 were converted to molar ellipticity using the following
166 equation:

$$167 \quad [\theta] = \frac{\text{deg}}{[c] \times \# \text{bonds} \times L \times 10000} \quad (1)$$

168 where deg is the raw signal in millidegrees, $[c]$ is protein
169 concentration in molar units, #bonds is the number of peptide
170 bonds, and L is the path length in centimeters.

171 **Folding Kinetics.** Fluorescence experiments were per-
172 formed in a Jasco FP-6500 spectrofluorometer. In all cases,
173 an excitation bandwidth of 1 nm and an emission bandwidth of
174 20 nm were used to minimize bleaching and to maximize the
175 signal-to-noise ratio. The temperature was controlled by a
176 Peltier device coupled to the measurement cell.

177 **Unfolding Kinetics.** Native protein from a concentrated
178 stock solution was diluted 10-fold by manual mixing into 10
179 mM Tris-HCl (pH 8.0), 200 mM NaCl, and 1 mM DTT buffer
180 with the indicated amount of Gdm.Cl, to a final protein
181 concentration of 8 μM . CD kinetics were monitored at 216 nm,
182 with a bandwidth of 10 nm and a response time of 4 s. A
183 decrease in the magnitude of the ellipticity signal was measured
184 until a steady state was reached. Fluorescence kinetics were
185 monitored by measuring NS1 fluorescence, originated by its
186 single tryptophan (Trp) residue, with an excitation wavelength
187 of 295 nm and an emission wavelength of 325 nm. The
188 fluorescence change (decrease) was measured until a steady
189 state was reached. In all experiments, the temperature was kept
190 constant at 20 $^{\circ}\text{C}$.

191 **Refolding Kinetics.** Unfolded NS1 from a concentrated
192 stock solution, equilibrated for at least 3 h in 5 M Gdm.Cl, was
193 diluted 10-fold by being manually mixed into 10 mM Tris-HCl
194 (pH 8.0), 200 mM NaCl, and 1 mM DTT buffer with the
195 indicated amount of Gdm.Cl, to a final protein concentration of
196 8 μM . Fluorescence kinetics were monitored with the same
197 parameters described for unfolding with a resultant increase in
198 Trp fluorescence.

199 **Stopped-Flow Kinetics.** Refolding kinetics were meas-
200 ured in a SX18MV stopped-flow apparatus (Applied Photo-
201 physics, Leatherhead, U.K.) by diluting equilibrated fully
202 unfolded protein from a concentrated (60 μM) stock solution
203 in 5 M Gdm.Cl, 10 mM Tris-HCl buffer (pH 8.0), 200 mM
204 NaCl, and 1 mM DTT 10-fold, into the same buffer with the
205 indicated amount of Gdm.Cl. The final protein concentration
206 throughout the experiments was 6 μM . The excitation
207 wavelength was 280 nm, and a 320 nm emission high-pass
208 filter was used.

209 **Folding Data Analysis.** The observed rate constants for
210 each folding or unfolding reaction were obtained by fitting the
211 kinetic traces, as required, to an equation containing up to three
212 exponential functions:

$$213 \quad F(t) = \sum A_n \exp(-k_n t) + F_{\infty} \quad (2)$$

214 where $F(t)$ and F_{∞} are the observed signal at time t and at
215 infinite time, respectively, and A_n and k_n are the signal
216 amplitude and rate constants, respectively, for each process.
217 Fitting was performed using the ProFit software (Quantumsoft,
218 Zurich, Switzerland). The criteria followed to choose the
219 minimal number of exponentials providing the best fit for each
220 trace were (1) a random dispersion of residuals, (2) low
221 standard deviation values (at most $1/5$ of the parameter value
222 for rate constants), and (3) significant improvement in the fit χ^2
223 values (in relation to an equation with simpler parameters).

When refolding data were being treated, three phases were
224 observed for all refolding reactions, in both slower time-scale
225 manual mixing and faster time-scale stopped-flow experiments.
226 As the slowest phase from stopped-flow experiments and the
227 fastest phase from manual mixing refolding experiments shared
228 similar rate constants, we performed a global fit of manual
229 mixing and stopped-flow refolding traces for most Gdm.Cl
230 concentrations tested. All traces were normalized prior to
231 fitting.

232 Following trace fitting, the natural logarithm of the observed
233 rate constants as a function of Gdm.Cl concentration was
234 plotted to obtain a chevron plot for NS1 folding. Assuming a
235 two-state model for NS1 folding, the following relationships
236 between equilibrium and kinetic constants can be obtained:
237



$$K_{\text{eq}} = k_f/k_u \quad (4) \quad 239$$

where U and N are the unfolded and native states, respectively,
240 K_{eq} is the folding equilibrium constant, and k_f and k_u are the
241 microscopic rate constants for folding and unfolding,
242 respectively.³⁰ K_{eq} for NS1 was previously reported, producing
243 a value of 6.48×10^{-8} .²⁸ The k_u was obtained from the chevron
244 plot, by extrapolating the value of $\ln k_{\text{obs}}$ at 0 M Gdm.Cl from a
245 linear fit of the unfolding limb, which showed a linear
246 dependence on Gdm.Cl concentration.³⁰ Using the two-state
247 model described in eqs 3 and 4, we calculated k_f from K_{eq} and
248 k_u . The m_{eq} value is a measure of the dependence of the free
249 energy of refolding on denaturant concentration³⁰ and was
250 previously reported for NS1, producing a value of 2.5 kcal
251 $\text{mol}^{-1} \text{M}^{-1}$.²⁸ The m_{eq} values were shown empirically to be
252 proportional to changes in accessible surface area (ΔASA) of
253 the native state of a protein upon unfolding.³¹ Similarly, kinetic
254 m values describe the dependence of the activation free energy
255 for folding and unfolding reactions on denaturant concen-
256 tration. The kinetic m_u^{\ddagger} value is considered to reflect changes in
257 ΔASA between the native state and the transition state
258 ensemble,³⁰ while the m_f^{\ddagger} value reflects changes in ΔASA
259 from the unfolded state to the transition state ensemble. The
260 m_u^{\ddagger} value was obtained from the chevron plot, as the slope of
261 the linear fit of the unfolding limb multiplied by RT , where R is
262 the gas constant ($1.9872 \times 10^{-3} \text{ kcal mol}^{-1}$) and T is the
263 temperature of the experiment in kelvin. Following the two-
264 state model, m_{eq} is related to m_f^{\ddagger} and m_u^{\ddagger} as follows³⁰
265

$$m_{\text{eq}} = m_u^{\ddagger} - m_f^{\ddagger} \quad (5) \quad 266$$

therefore, we calculated m_f^{\ddagger} using eq 5 and the obtained values
267 of m_{eq} and m_u^{\ddagger} . To gain information about the burial of
268 accessible surface area in the transition state, we calculated an α
269 value, as follows:³²
270

$$\alpha = 1 - \frac{m_u^{\ddagger}}{m_{\text{eq}}} \quad (6) \quad 271$$

Oligomerization Kinetics. Oligomerization was followed
272 by monitoring changes in the far-UV CD signal at 220 nm or in
273 thioflavin T fluorescence following transfer of monomeric NS1
274 from a concentrated stock solution held at 4 $^{\circ}\text{C}$ to a cuvette
275 containing 10 mM Tris-HCl buffer (pH 8.0) and 1 mM DTT,
276 maintained at the indicated temperature in each experiment.
277 The concentration dependence of the reaction was measured
278

by varying the NS1 concentration from 2.5 to 10 μM at 47 $^{\circ}\text{C}$. The oligomerization reaction was additionally measured by following the increase in ThT fluorescence with time after concentrated NS1 was transferred to a cuvette containing buffer equilibrated with a final ThT final concentration of 20 μM . We previously showed that monomeric NS1 does not bind ThT while NS1 oligomers do bind ThT.²⁸ Therefore, the ThT fluorescence increase was used as a proxy of NS1 oligomerization. The excitation wavelength in these experiments was 446 nm, and signal changes were monitored at 490 nm, using an excitation bandwidth of 1 nm and an emission bandwidth of 20 nm.

Dynamic Light Scattering. The particle size distribution for NS1 samples was obtained using a Zetasizer Nano S DLS device from Malvern Instruments (Malvern). NS1 protein was filtered with Ultrafree-MC microcentrifuge 0.22 μm filters (Millipore) before measurements were taken. NS1 protein at 17 μM in buffer containing 10 mM Tris-HCl with 1 mM DTT was incubated at 40 $^{\circ}\text{C}$ (controlled by a Peltier control system), and time-dependent changes in particle size diameter were followed. Each measurement was an average from 10 scans of 10 s each.

Temperature-Jump Experiments. NS1 from a stock solution held at 4 $^{\circ}\text{C}$ was transferred to 10 mM Tris-HCl buffer (pH 8.0) and 1 mM DTT at 47 $^{\circ}\text{C}$ with a final protein concentration of 12 μM . After a delay time ranging from 50 to 2000 s, samples were transferred to a sample cell holder kept at 20 $^{\circ}\text{C}$ and the far-UV CD signal at 220 nm was monitored. After a steady state had been reached, far-UV CD spectra were measured, and samples were run in a gel filtration S-75 column.

Size Exclusion Chromatography. Size exclusion chromatography experiments were conducted on a Superdex 75 HR 10/30 column (24 mL) at a flow rate of 0.5 mL/min. The column was calibrated with ovalbumin (44.2 kDa), chymotrypsinogen A (25 kDa), and ribonuclease A (13.7 kDa). The void volume (V_0) and total volume (V_t) were determined by loading blue dextran and acetone, respectively. The buffer consisted of 10 mM Tris-HCl (pH 8.0) and 1 mM DTT with a protein concentration of 12 μM at 20 $^{\circ}\text{C}$.

Oligomerization Data Analysis. Traces from concentration dependence experiments were normalized and used for model analysis. For the determination of nucleus size, we used a kinetically limited model, developed by Zlotnick et al.:³³

$$\log[\text{NSISOs}] = \log k + n \times \log[\text{NS1}_{\text{monomer}}] \quad (7)$$

where k is a proportionality constant and n is the size of the nucleus. The ThT fluorescence was used as a proxy of NSISOs assembly. $[\text{NSISOs}]$ and $[\text{NS1}_{\text{monomer}}]$ represent the concentration of NS1 oligomers and monomers, respectively, and were calculated at five different time points during the exponential phase (ranging 200 to 600 s). At each time point and concentration, we defined $[\text{NSISOs}] = [\text{NS1 total concentration}](\text{normalized ThT fluorescence signal})$ and $[\text{NS1 monomer}] = [\text{NS1 total concentration}](1 - \text{normalized ThT fluorescence signal})$. These parameters were used to create a log–log plot. The size of the nucleus was then estimated from averaging the slope of the log–log plot of $[\text{NSISOs}]$ versus $[\text{NS1 monomer}]$ for all curves. The obtained value was an average of the values obtained from the different time-point data sets analyzed. The elongation rate constant for each trace was determined from the slope of the traces centered at 25% signal saturation. The order of the assembly reaction

was determined from the slope of a log–log plot of the rate constants versus total NS1 concentration, as follows:

$$\log(\text{elongation rate}) = l \times \log[\text{NS1}_{\text{total}}] + C \quad (8)$$

where $[\text{NS1}_{\text{total}}]$ is the NS1 total concentration, l is the order of the reaction, and C is a constant.³⁴

RESULTS

NS1 Shows a Simple Unfolding Kinetics. We previously showed that NS1 unfolds in a highly cooperative manner at

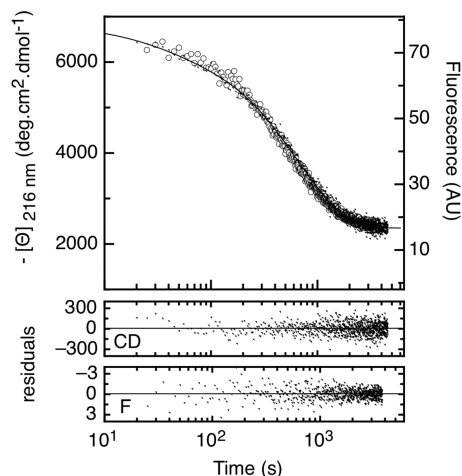


Figure 1. NS1 unfolding kinetics. Unfolding kinetics of native NS1 protein diluted 10-fold to a final concentration of 8 μM , following changes in far-UV CD and fluorescence signals at 5.0 M Gdm.Cl. The far-UV CD signal was followed at 216 nm, and the fluorescence signal was followed at 325 nm. Traces were fit to a monoexponential function (solid line) with residuals from the fit shown below the graph. The observed rate constants obtained from fitting were $(1.80 \pm 0.2) \times 10^{-3} \text{ s}^{-1}$ from fluorescence experiments and $(1.6 \pm 0.2) \times 10^{-3} \text{ s}^{-1}$ from CD experiments.

equilibrium, following a two-state and fully reversible reaction characterized by a concomitant loss of secondary and tertiary structure, with $\Delta G^{\text{H}_2\text{O}}_{\text{N-U}}$ and m_{eq} values of $9.6 \pm 0.9 \text{ kcal mol}^{-1}$ and $2.5 \text{ kcal mol}^{-1} \text{ M}^{-1}$, respectively.²⁸ As part of the dissection of the folding mechanism, we tackled a kinetic investigation. We started by studying NS1 unfolding kinetics by following changes in exposure of its single solvent-protected tryptophan residue (indicative of global tertiary structure unfolding), and also by monitoring changes in NS1 secondary structure upon Gdm.Cl denaturation through far-UV circular dichroism (CD) measurements. As unfolding was a slow process, we performed manual mixing experiments in which native NS1 from a concentrated stock solution was diluted 10-fold into buffer solutions containing Gdm.Cl at a final concentration ranging between 3.75 and 7.0 M (pH 8.0), and followed the resulting kinetic signals over time (see [Experimental Procedures](#)).

Unfolding proved to be a rather simple process at all Gdm.Cl concentrations tested, and data analysis showed that at low and moderate Gdm.Cl concentrations (from 3.75 to 7.0 M) unfolding traces could be fitted to a single-exponential function (Figure 1 and Figures 1 and 2 of the Supporting Information). At 5.0 M Gdm.Cl, the observed rate constant was $(1.80 \pm 0.02) \times 10^{-3} \text{ s}^{-1}$, indicating a half-life of ~ 6 min for the unfolding reaction. The presence of a single observed rate constant in this

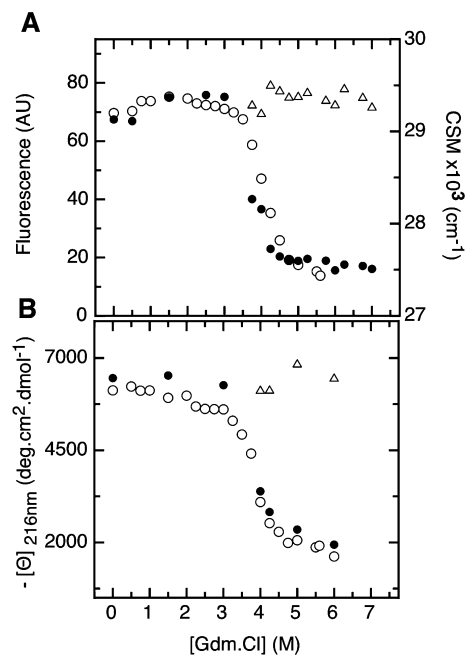


Figure 2. Amplitude analysis for NS1 unfolding. Initial [$t = 0$ (Δ)] and final [$t = \infty$ (\bullet)] signals from kinetic unfolding experiments followed by (A) fluorescence or (B) the CD signal at 216 nm. In both graphs, final signals were calculated as the end point of exponential fits while initial values were calculated as the difference between the end-point values and the total amplitudes from all phases obtained in data fitting. The data from equilibrium unfolding experiments reported in ref 28 followed by the Trp fluorescence center of spectral mass (CSM) and by the far-UV CD signal at 216 nm are shown superimposed on amplitude data in panels A and B, respectively (\circ).

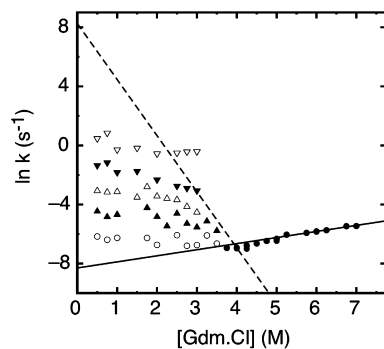


Figure 3. Chevron plot for NS1 folding. Gdm.Cl dependence of the rate constants from unfolding and refolding experiments (chevron plot) shown in Figures 1 and 2 and Figures 1–5 of the Supporting Information. The rate constants corresponding to the unfolding phase from fluorescence measurements are represented as black circles for fluorescence measurements and as gray circles for CD measurements. The five observed refolding phases obtained by global data fitting are shown in the refolding side of the plot from 0 to 3.5 M Gdm.Cl (∇ , \blacktriangledown , Δ , \blacktriangle , and \square). The solid line represents a linear fit of the unfolding phase from 5.0 to 7.0 M Gdm.Cl. k_u was obtained from extrapolation of the value of $\ln k_u$ at 0 M Gdm.Cl, producing a value of $(2.5 \pm 0.5) \times 10^{-4} \text{ s}^{-1}$, and m_u^\ddagger was obtained from the slope of the graph multiplied by RT ($0.582 \text{ kcal mol}^{-1}$), producing a value of $0.24 \pm 0.02 \text{ kcal mol}^{-1} \text{ M}^{-1}$. The dashed line represents the predicted linear fit for the major refolding phase, obtained by assuming a two-state folding model (see eqs 4 and 5 of Experimental Procedures), which yielded a value of $3860 \pm 850 \text{ s}^{-1}$ for k_f and a value of $-2.26 \pm 0.20 \text{ kcal mol}^{-1} \text{ M}^{-1}$ for m_f^\ddagger .

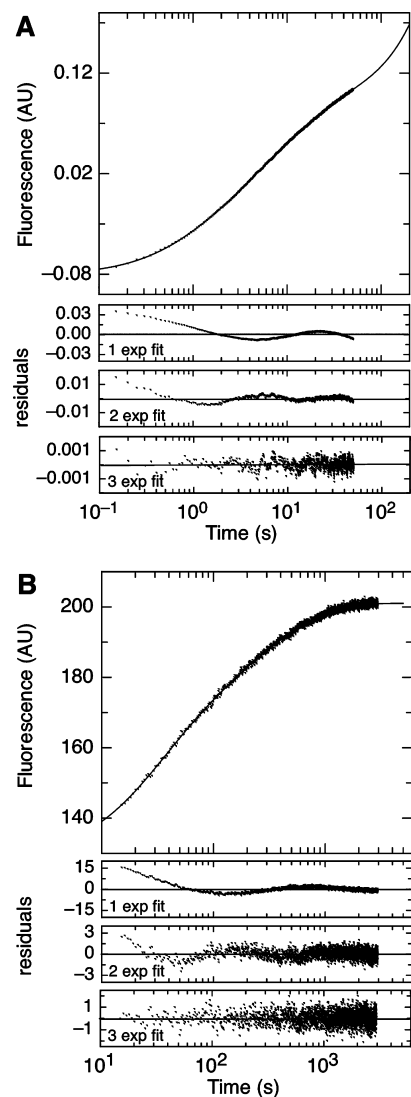


Figure 4. NS1 refolding kinetics. Unfolded NS1 was rapidly mixed in buffer to a final Gdm.Cl concentration of 1 M, and the Trp fluorescence intensity change was monitored. (A) NS1 refolding kinetics followed by a stopped-flow method. The final protein concentration was $6 \mu\text{M}$. (B) Refolding kinetics followed by manual mixing. The final protein concentration was $8 \mu\text{M}$. The mixing dead time of the experiment was 15 s. For both experiments, traces were fitted to single-, double-, and triple-exponential functions (dashed line), with residuals for each fit shown below each trace. The observed rate constants for panel A were as follows: $k_1 = 1.5 \pm 0.1 \text{ s}^{-1}$, $k_2 = 0.32 \pm 0.01 \text{ s}^{-1}$, and $k_3 = (7.0 \pm 0.3) \times 10^{-2} \text{ s}^{-1}$. For panel B, the observed rate constants were as follows: $k_4 = (3.8 \pm 0.2) \times 10^{-2} \text{ s}^{-1}$, $k_5 = (8.5 \pm 0.5) \times 10^{-3} \text{ s}^{-1}$, and $k_6 = (1.9 \pm 0.1) \times 10^{-3} \text{ s}^{-1}$.

Table 1. Observed Rate Constants Obtained from Refolding Experiments at 1.0 M Gdm.Cl

	constant (s^{-1})	error (s^{-1})
k_1	0.7451	3.33×10^{-2}
k_2	0.1604	7.07×10^{-3}
k_3	0.0434	2.34×10^{-3}
k_4	0.0093	3.68×10^{-4}
k_5	0.0019	2.70×10^{-5}

Gdm.Cl concentration range indicated that only two species 373 were populated in the unfolding reaction, the native state and 374

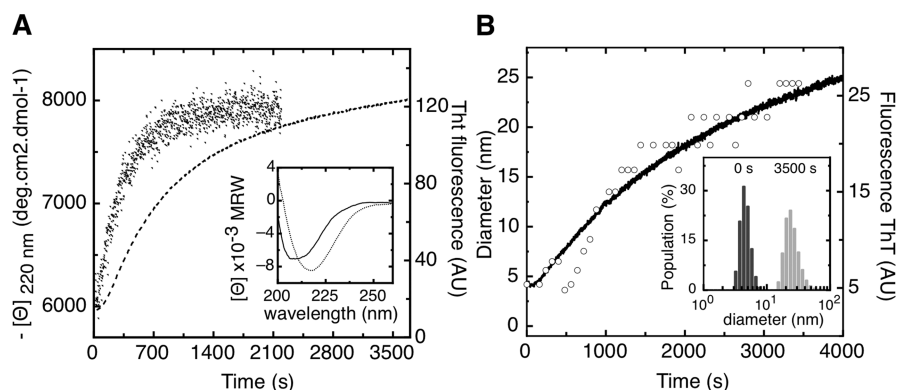


Figure 5. Kinetics of NS1SOs formation by temperature jump. (A) Oligomerization kinetics were measured after transferring concentrated native NS1 from 4 °C to buffer equilibrated at 47 °C, and following changes in the far-UV CD signal at 216 nm (black dots) and in ThT fluorescence (dashed line) in two independent experiments. The final NS1 concentration in both experiments was 10 μ M. The inset shows the far-UV CD spectra of native NS1 (solid) and NS1SOs at the end point of the experiment (dashed line). (B) Native NS1 held at 4 °C was transferred to a cell holder maintained at 40 °C at a final concentration of 17 μ M, and the resulting kinetics were measured by following changes in the particle size diameter by DLS (O) and by following the increase in ThT fluorescence (black line) in two independent experiments. The inset shows the particle size distribution, measured by DLS, of initial and final species.

the unfolded state. For all Gdm.Cl concentrations tested, changes in secondary and tertiary structure were superimposable processes and yielded similar rate constants (Figure 1). As an example, at 6.0 M Gdm.Cl, data fitting yielded the following rate constants for unfolding: $(2.89 \pm 0.02) \times 10^{-3}$ and $(2.97 \pm 0.02) \times 10^{-3} \text{ s}^{-1}$ for fluorescence and CD experiments, respectively.

The amplitudes and end points of the observed rate constants, from data fitting for fluorescence and CD unfolding experiments, were used to create a plot of initial and final values of the signals (Figure 2A,B). This analysis showed an excellent superposition between equilibrium and kinetic unfolding data and also indicated that the observed amplitudes could account for the full change in each signal. These results indicate the absence of rapid processes (burst phase) during the experimental mixing dead time. The observed rate constants from fluorescence experiments as a function of Gdm.Cl concentration were plotted to create a chevron plot. For unfolding, we observed a linear dependence of the logarithm of the observed rate constant on guanidinium concentrations for most of the concentrations tested (Figure 3). We calculated the unfolding rate constant (k_u) at 0 M Gdm.Cl by extrapolation of a linear regression of the observed rate constants (from 5.0 to 7.0 M Gdm.Cl), producing a value of $(2.5 \pm 0.5) \times 10^{-4} \text{ s}^{-1}$, and a value of $0.24 \pm 0.02 \text{ kcal mol}^{-1} \text{ M}^{-1}$ for m_u^\ddagger (Figure 3; see Experimental Procedures).

NS1 unfolding can thus be described as a slow single-exponential decay that accounts for the full change in fluorescence and CD signal between the native and unfolded states. Kinetics recorded by CD and fluorescence are superimposable at all Gdm.Cl concentrations tested, and the Gdm.Cl dependence of the logarithm of the observed rate constant is linear. From this evidence, we can describe NS1 unfolding as a two-state process without populated intermediates.

Complex Multiphasic Refolding Kinetics. Refolding was initially investigated by manual mixing and stopped-flow techniques as it proved to be a multiphasic process with both several slow phases (minute time scale) and rapid phases (second time scale) that could not be measured by manual mixing (15 s). For both sets of experiments, concentrated and unfolded protein was diluted 10-fold in the appropriate buffer

to reach final Gdm.Cl concentrations ranging from 0.5 to 3.5 M. In both cases, the refolding process was followed by measuring changes in Trp fluorescence (see Experimental Procedures).

Traces from stopped-flow experiments performed at 1 M Gdm.Cl were best fitted to three exponential functions (Figure 4A), as was the case for most of the Gdm.Cl concentrations tested (see Figure 3 of the Supporting Information). Fitting of kinetic data from manual mixing experiments at 1 M Gdm.Cl also showed the presence of three phases (Figure 4B), as did most of the Gdm.Cl concentrations tested (see Figure 4 of the Supporting Information). As a result, data yielded six observed rate constants. At all Gdm.Cl concentrations tested, the slowest phase measured by stopped-flow techniques had a rate constant similar to that of the fastest phase measured by manual mixing experiments. For example, at 1.0 M Gdm.Cl, these phases yielded the following rate constants: $k_3 = (7.0 \pm 0.3) \times 10^{-2} \text{ s}^{-1}$ for stopped-flow experiments, and $k_1 = (3.8 \pm 0.2) \times 10^{-2} \text{ s}^{-1}$ for manual mixing experiments, which indicated that this phase corresponded to the same event. We performed a global fit of the stopped-flow and manual mixing refolding data (see Experimental Procedures and Figure 5 of the Supporting Information), and on the basis of this analysis, five phases could be well discriminated, with observed rates ranging from $0.75 \pm 0.03 \text{ s}^{-1}$ for the fastest phase to $(1.90 \pm 0.27) \times 10^{-3} \text{ s}^{-1}$ for the slowest phase at 1.0 M Gdm.Cl (Table 1). The presence of five phases indicated the population of at least four intermediate species in the refolding process.^{30,35}

The amplitude analysis from refolding experiments was not performed because of the instability of the stopped-flow fluorescence signal to obtain a baseline of the native and unfolded states. Therefore, the absence of a burst phase in the folding reaction could not be established. The resulting chevron plot from refolding experiments revealed that most phases presented a very weak dependence on Gdm.Cl concentration (Figure 3), suggesting that they do not appear to represent major folding events. Remarkably, despite the fact that NS1 was previously found to undergo oligomerization under mild changes in solvent conditions,²⁸ we found no dependence on protein concentration for either of the refolding rates [assessed in the range of 1–15 μ M for manual mixing and in the range of

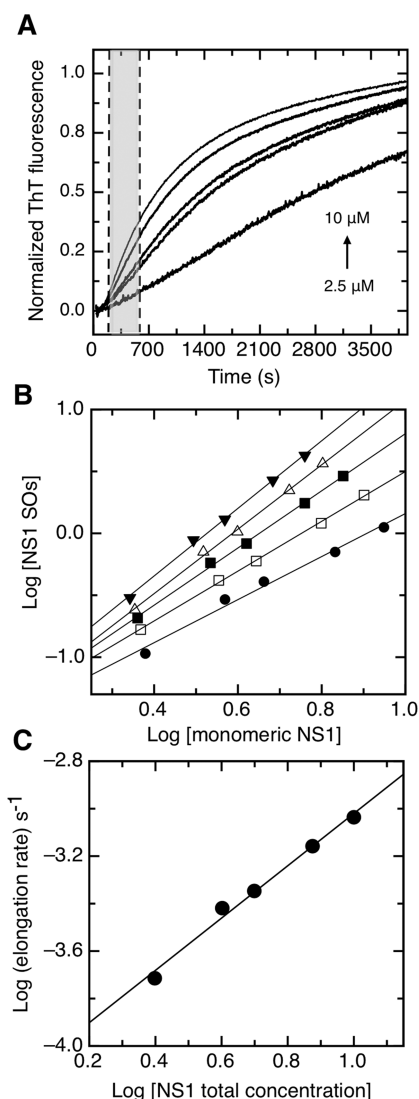


Figure 6. Kinetics and concentration dependence of NS1 self-assembly. (A) Normalized ThT fluorescence signals at NS1 protein concentrations ranging from 2.5 to 10 μM (from bottom to top, respectively). The gray area indicates the range of time points used for nucleus size analysis. (B) Log–log plot of NS1SOs concentration as a function of monomeric NS1 concentration. Each data set of values was calculated using data from all protein concentration at different time points within the gray zone demarked in panel B: 200 (●), 300 (◇), 400 (■), 500 (△), and 600 s (▼). The nucleus size (2.3 ± 0.3) was calculated as an average of the slopes obtained for each data set according to eq 7 (see Experimental Procedures). (C) The reaction order for NS1SOs formation was calculated from the slope of the power dependence of the elongation rate as a function of NS1 total concentration according to eq 8 (see Experimental Procedures), producing a value of 1.10 ± 0.06 .

steps in NS1 refolding could be due to Xaa-prolyl isomerization of one or more of its four proline residues,^{37–39} although further experiments are needed to confirm this hypothesis.

Kinetic Dissection of NS1 Oligomerization. We have previously shown that NS1 readily forms soluble and well-defined oligomers (NS1SOs) upon mild modifications in the milieu.²⁸ NS1SOs formation is accompanied by a substantial change in NS1 secondary structure, with an increase in β -sheet content (Figure 5A, inset).²⁸ Moreover, NS1SOs were found to share features with amyloid-like or repetitive β -sheet structures, such as thioflavin T and Congo red binding.²⁸ To investigate the mechanism of this quasi-spontaneous NS1 oligomerization pathway, we performed a kinetic study using ThT fluorescence, dynamic light scattering (DLS), and CD.

NS1 was stable at 20 °C, whereas transfer to temperatures of >40 °C led to NS1SOs formation (Figure 5). The formation of NS1SOs was triggered by a temperature jump. In a first experiment, the assembly process was monitored by the increase in ThT fluorescence with time, after native NS1 held at 4 °C was transferred to a buffer solution equilibrated at 40 °C. A slow increase in the level of ThT binding was observed, indicative of the formation of quaternary structure containing repetitive β -strands (Figure 5A). In a parallel experiment, we used DLS to monitor the particle size diameter of native NS1 held at 4 °C after transfer to a cell holder maintained at 40 °C [Figure 5B (○)]. The initial species showed an average particle size diameter of 4.2 nm, and at the end point of the kinetics, the particle size diameter was 24.4 nm, in excellent agreement with the previously described monomeric and oligomeric species²⁸ (Figure 5B, inset). The process showed multiple phases, with a noticeable lag phase that preceded the increase in ThT fluorescence within the first 100 s. This lag phase was also evident when monitoring the particle size increase by DLS as the reaction proceeded, indicating the presence of intermediate species prior to oligomer formation (Figure 5B). Interestingly, far-UV CD showed that changes in NS1 secondary structure took place before oligomer formation (Figure 5A), further supporting the presence of intermediate protein concentration-independent species in the oligomerization process.

Defining Nucleation and Elongation Steps in NS1SOs Assembly. Next, to further dissect the mechanism of NS1 oligomerization, we analyzed time-dependent changes in ThT fluorescence at varying protein concentrations, where native NS1 held at 4 °C was transferred to buffer equilibrated at 47 °C, and the resulting kinetics was measured by the increase in ThT fluorescence. The temperature was chosen to optimize the time window for data analysis, with protein concentrations ranging from 2.5 to 10 μM (Figure 6A). Normalization of the data showed protein concentration-dependent kinetics, as expected for a polymerization reaction (Figure 6A). To characterize the process, we used an oligomerization model developed by Zlotnick et al.³³ used to describe sigmoidal assembly kinetics in which there are three well-defined phases, namely, a lag phase, an elongation phase, and a final stationary phase. In this model, the lag phase can be correlated to nucleus formation, where the nucleus is defined as the minimal assembly unit.⁴⁰ The ThT fluorescence kinetic data were normalized and used as an estimate of NS1SOs concentration (Figure 6A). At different time points during the exponential phase (Figure 6A, gray zone), the NS1SOs concentration and NS1 monomer concentration for all concentrations tested were calculated (Figure 6B). The log–log plot of NS1SOs concentration as a function of NS1 monomer concentration

1–10 μM for stopped-flow experiments (not shown)], indicating that they did not reflect oligomerization events.

Taken together, these experiments allow us to conclude that, unlike unfolding, refolding is a complex reaction limited by slow unimolecular processes whose rates display a weak dependence on guanidinium concentration. The values of the rate constants, together with their weak Gdm.Cl dependence, are compatible with the rates associated with prolyl isomerization in the unfolded state, which are within the range of 0.001–0.1 s^{-1} .³⁶ This suggests that the observed rate-limiting

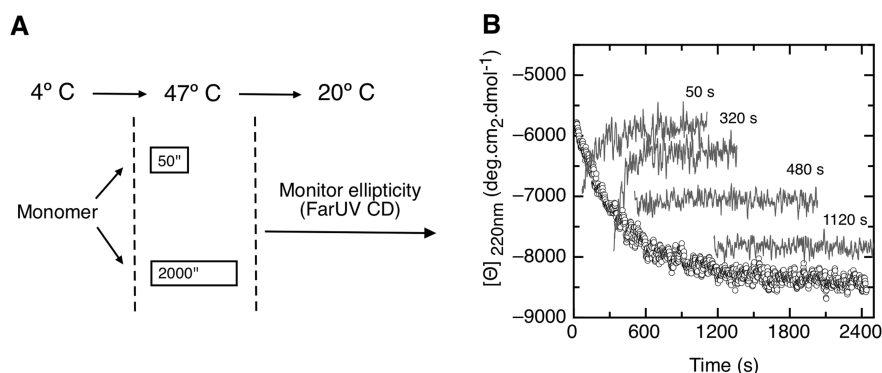


Figure 7. Double-temperature-jump experiments. (A) Native NS1 held at 4 °C was transferred to buffer equilibrated at 47 °C at a final concentration of 12 μ M. At different time points from 50 to 2000 s, the samples were transferred to a cell holder equilibrated at 20 °C and the ensuing kinetics were measured following changes in the far-UV CD ellipticity. In a similar experiment, NS1 oligomer formation was detected by size exclusion chromatography (Figure 8). (B) Oligomerization kinetics measured by far-UV CD ellipticity at 220 nm (white dots). The solid lines at 50, 320, 480, and 1120 s represent the changes in the far-UV CD signal kinetics upon cooling from 47 to 20 °C.

allows for nucleus size determination (Figure 6B; see Experimental Procedures), where we calculated a nucleus size of 2.3 ± 0.3 NS1 molecules as an average value from the slope of five different time-point data sets. These results indicated that the nucleus for NS1 oligomerization is a dimeric species. In addition, the order of the elongation reaction was determined from the slope of the log–log plot of the rate of NS1SOs formation as a function of NS1 total concentration (Figure 6C; see Experimental Procedures). A value of 1.10 ± 0.06 NS1 molecules was obtained, clearly indicative of a first-order reaction, where oligomerization proceeds, through addition of monomers to the dimeric nucleus.

Partial Reversibility of Intermediate Stages in NS1SOs Assembly. As we previously described, the overall oligomerization reaction is an irreversible process.²⁸ However, an important goal is to determine when this irreversibility takes place, and which intermediate events in NS1SOs assembly remain reversible. We tackled this issue by performing a double-temperature-jump experiment in which native NS1 was transferred to 47 °C and at different time intervals the oligomerization reaction was stopped by transfer to 20 °C while far-UV CD ellipticity was monitored at 220 nm (Figure 7A). The oligomerization process was characterized by an increment in negative ellipticity at 220 nm, from -5500 to -8500 deg cm² dmol⁻¹ (Figure 7B). Interestingly, we found that at short time delays cooling back led to recovery of the initial ellipticity signal, yielding steady state values equal to those of the NS1 monomer. The final species obtained at the end point after the temperature jump at 50 s had a far-UV CD spectrum identical to that of native NS1 (Figure 8A), indicating that at early stages the oligomerization process was reversible. At longer time delays, this reversibility was slowly lost, as indicated by a lack of full recovery of the CD signal, which takes place between 320 and 480 s (Figure 7B). To verify these results, we performed a similar experiment in which the oligomerization state of the final species formed was monitored using size exclusion chromatography, performed at the end of each experiment after transfer back to 20 °C (Figures 7A and 8B). At 50 and 100 s delays, we did not detect significant oligomer formation, confirming the full reversibility of the process as observed by CD, and monomeric native NS1 was recovered. In agreement with the CD kinetics experiment, there was a gradual accumulation of oligomeric species that eluted in the void volume of the column after transfer back to 20 °C at longer

time delays, and this accumulation proved to be highly superimposable with the oligomerization reaction followed by ThT fluorescence (Figure 8C).

DISCUSSION

The NS1 protein from human respiratory syncytial virus is considered one of the main RSV virulence factors, having a central role in innate immunity inhibition. Despite its relevance, little is known about the molecular mechanisms involved in this immune evasion process. In addition, the absence of an effective vaccine or antiviral treatment shows the need for detailed mechanistic information because biophysical information is scarce and the structure and biophysical properties of this protein have not been elucidated to date. Previously, we showed that NS1 can populate several conformational states at equilibrium, including the native and unfolded monomers, and spherical oligomeric species.²⁸ To characterize the dynamics of interconversion among these species, we performed kinetic measurements of folding and temperature-induced oligomerization.

Figure 9 shows a summary of NS1 diverse stable species in solution, and the transitions between them. Kinetic unfolding of native state N is a two-state process with a half-time of 46 min, which indicates a high kinetic stability of the native monomer. In addition, the denaturant dependence of the unfolding kinetics and equilibrium allow us to characterize the transition state for the unfolding reaction. We used the corresponding m values to calculate an α value [$\alpha = 1 - m_u/m_{eq}$] (see Experimental Procedures).^{31,32} The α value can be interpreted as the relative amount of accessible surface area in the transition state ensemble. In the simplest case, this parameter takes values between 0 and 1, where 1 indicates a nativelike accessible surface area in the transition state and 0 indicates an unfolded-like accessible surface area in the transition state. We obtained an α value of 0.90 ± 0.02 , indicative of a transition state ensemble for unfolding with nativelike solvent accessibility.

On the basis of our refolding experiments, we propose a minimal model for NS1 folding (Figure 9, left-hand side). According to this model, formation of a folding-competent species (U_{Fast}), which has all its Xaa-proline residues in their yet unknown native conformation, is limited by slow equilibria with unfolded NS1 monomers containing one or more non-native prolyl isomers (U_{Slow} species). Assuming that the four NS1

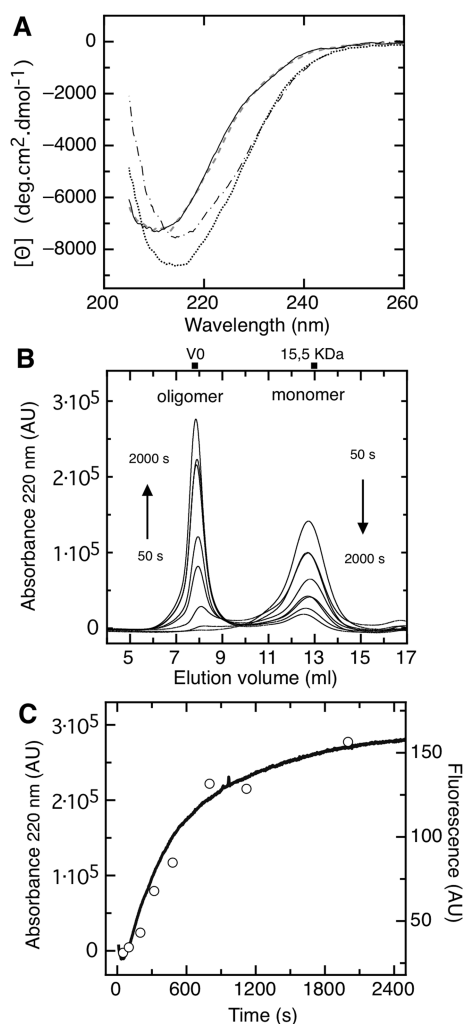


Figure 8. Reversible stage in oligomer formation determined by double-temperature-jump experiments. (A) Far-UV CD spectra for samples from Figure 7: native NS1 (solid line) and samples measured at the end point of the kinetics after they had been cooled at 20 °C for 50 s (dashed line), 480 s (dashed and dotted line), and 1120 s (dotted line). (B) Size exclusion chromatography (SEC) of samples heated at 47 °C and cooled at different time points (between 50 and 2000 s) of the oligomerization process, as shown in Figure 7. SEC oligomerization experiments were performed after the samples had been cooled at 20 °C. The void volume of the column was 8.0 mL, and the expected elution volume for a 15.5 kDa protein according to a calibration with protein standards is 13.0 mL. (C) Maximal observed absorbance values at 220 nm of particles eluted in the void volume (○) superimposed on the ThT fluorescence increase (—).

very short half-life (0.2 ms) and rapidly yields the native state N.

The right-hand side of Figure 9 shows a model for NS1SOs assembly. Oligomerization kinetics follow a sequential process, in which the main events are represented by a lag phase, an elongation phase, and a stationary phase (Figure 5), features that are typical of nucleation-limited polymerization reactions. During the lag phase, no oligomers are formed (Figure 5B), but substantial secondary structure changes in the native NS1 monomer N take place on a time scale of minutes (Figure 5A) to form a non-native monomer M* (Figure 9). Data fitting from CD experiments at 10 μM using a single-exponential decay allowed us to estimate the time constant of this step, yielding a half-time of 3.8 min (Figure 9). During the lag phase, conformational changes are reversible, and the native monomer N can be recovered upon cooling (Figures 7 and 8). After the dimeric nucleus M2* is formed during the lag phase, most if not all of the secondary structure change has taken place (Figures 5A and 6B). This event is followed by the sequential addition of monomers (Figures 6C and 8), which becomes irreversible between 320 and 480 s at a protein concentration of 10 μM (Figure 7B). Under these conditions at 47 °C, NS1SOs assembly is complete within 83 min (Figure 6A). Using the estimated number of monomers in NS1SOs of 149,²⁸ we estimate that during polymerization one NS1 monomer will be added on average to the oligomer every 34 s (Figure 9).

Previous work has described the presence of NS1 oligomers in transfected and infected cells as well as large functional complexes with other proteins.^{20,29} For example, the RSV NS degradosome was shown to be heterogeneous in size (300–750 kDa) and proposed to include the viral NS1 and NS2 proteins as well as host proteasome subunits. The size of the degradosome is compatible with the presence of NS1 oligomers within it. Suppression of the innate immune response in HRSV-infected cells is mediated by interactions between the NS degradosome and a large oligomeric assembly of MAVS proteins on the mitochondrial membrane, which enhances viral degradative activity.²⁹ The mitochondrial signaling protein (MAVS) oligomerizes following viral infection, forming active amyloid type polymers that amplify IFN signaling.⁸ Moreover, electron microscopy studies showed that NS1 and MAVS colocalize, suggesting that both proteins may mediate the interaction between the NS degradosome and the MAVS assembly.²⁴ If this is the case, NS1 oligomerization may act as a scaffold for degradosome assembly as well as for interaction with MAVS, making NS1 oligomerization a plausible drug target for suppressing viral shutdown of the host innate immune response.

In summary, here we describe diverse but discrete states of RSV NS1 in solution that may help us understand its multiple reported binding activities,^{20–22} especially so in the absence of structural information, homologues, or functionally related proteins within paramyxoviruses. These multiple binding activities must be accommodated in a few binding interfaces at most, something unlikely to be specific given its small size (15 kDa). This strongly suggests that conformational heterogeneity, and in particular oligomer formation, may provide a necessary means of expanding the NS1 binding repertoire.

The different species described herein interconvert on a time scale of minutes to hours, implying that even if they are present at low concentrations, variables such as macromolecular crowding, protein–protein interactions, or specific subcellular

prolines populate the *trans* isomer in the native state, statistically at least 35% of unfolded molecules would present a non-native peptide bond at equilibrium.³⁶ If one of the prolines populates the *cis* isomer in the native state, this percentage would increase to 92%.³⁶ The question of whether NS1 molecules with non-native peptide bonds can fold or function to a significant degree remains intriguing. We may also consider the folding rate of the folding-competent U_{Fast} species. We estimated the value of the main refolding rate constant by combining data measured from unfolding kinetics with previously reported equilibrium data.²⁸ This yielded a *k_f* value of 3860 ± 850 s⁻¹ and an *m_f[‡]* value of -2.26 ± 0.20 kcal mol⁻¹ M⁻¹ (Figure 3 dashed line; see Experimental Procedures), indicating that the highly competent U_{Fast} folding species has a

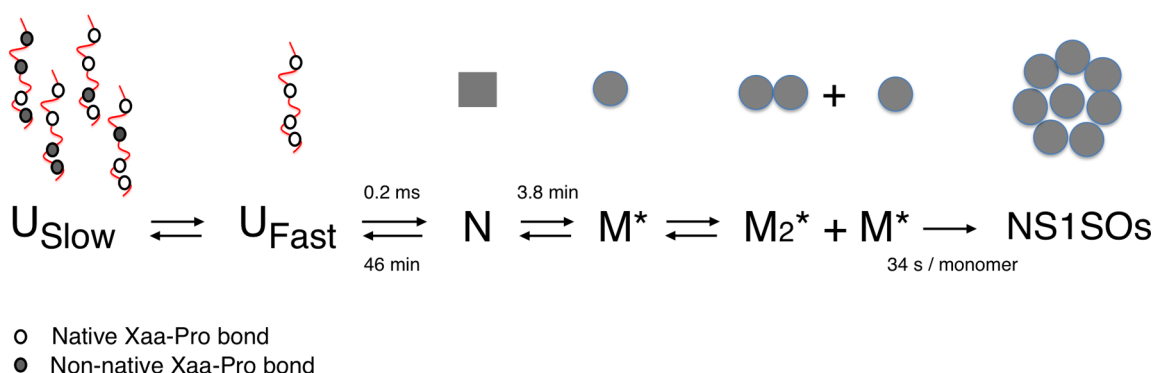


Figure 9. Minimal model for NS1 folding and NS1SOs formation. The diagram represents the proposed minimal model for NS1 folding and oligomerization, where U_{Slow} species are unfolded polypeptides with non-native Xaa-prolyl isomers (●), U_{Fast} is the unfolded polypeptide chain with native Xaa-prolyl isomers (○), and N is the native NS1 monomer. In the polymerization reaction, M^* represents a native-like monomer and M_2^* is the dimeric nucleus for formation of the NS1 spherical oligomers (NS1SOs), which proceeds via addition of the monomer to the dimeric nucleus. In the model, two-way arrows indicate reversible processes while one-way arrows indicate irreversible reactions. The half-times for folding, unfolding, and oligomer formation obtained from kinetic analysis are reported.

localization may alter the equilibria and dynamics of these processes leading to their accumulation. The irreversible and quasi-spontaneous nature of NS1SOs assembly under mild temperature conditions, together with the fact that it is the most abundant viral protein in RSV-infected cells, makes its accumulation highly conceivable. This work should be extended to the investigation of oligomers in infected cells and their functional implications for the viral life cycle and for the inhibition of the host innate immune response.

ASSOCIATED CONTENT

Supporting Information

The Supporting Information is available free of charge on the ACS Publications website at DOI: 10.1021/acs.biochem.5b00615.

Supplementary Figures S1–S5 (PDF)

AUTHOR INFORMATION

Corresponding Author

*E-mail: gpg@leloir.org.ar.

Funding

This work was supported by ANPCyT (Agencia Nacional de Promoción Científica y Tecnológica) PICT 2011-0721, CONICET (Consejo Nacional de Investigaciones Científicas y Técnicas) PIP 2011-2014, and Ciência Sem Fronteiras (Rio de Janeiro, Brazil) Program Grants to G.d.P.-G. E.P. and M.F. are recipients of a CONICET predoctoral fellowship, and I.E.S., L.B.C., and G.d.P.-G. are CONICET researchers.

Notes

The authors declare no competing financial interest.

ABBREVIATIONS

RSV, respiratory syncytial virus; hRSV, human respiratory syncytial virus; IFN, interferon; NS1SOs, NS1 soluble spherical oligomers; CD, circular dichroism; ThT, thioflavin T.

REFERENCES

(1) Lamb, R. A., and Parks, G. D. (2007) Paramyxoviridae: The viruses and Their Replication. In *Fields in Virology* (Knipe, D. M., and Howley, P. M., Eds.) Vol. 1, Chapter 41, pp 1449–1496, Lippincott Williams & Wilkins, Philadelphia.

(2) Welliver, R. C. (2004) Respiratory syncytial virus infection: therapy and prevention. *Paediatr Respir Rev.* 5 (Suppl. A), S127–S133.

(3) Jafri, H. S., Chavez-Bueno, S., Mejias, A., Gomez, A. M., Rios, A. M., Nassi, S. S., Yusuf, M., Kapur, P., Hardy, R. D., Hatfield, J., Rogers, B. B., Krisher, K., and Ramilo, O. (2004) Respiratory syncytial virus induces pneumonia, cytokine response, airway obstruction, and chronic inflammatory infiltrates associated with long-term airway hyperresponsiveness in mice. *J. Infect. Dis.* 189, 1856–1865.

(4) Empey, K. M., Peebles, R. S., Jr., and Kolls, J. K. (2010) Pharmacologic advances in the treatment and prevention of respiratory syncytial virus. *Clin. Infect. Dis.* 50, 1258–1267.

(5) Collins, P. L., and Melero, J. A. (2011) Progress in understanding and controlling respiratory syncytial virus: still crazy after all these years. *Virus Res.* 162, 80–99.

(6) Myong, S., Cui, S., Cornish, P. V., Kirchhofer, A., Gack, M. U., Jung, J. U., Hopfner, K. P., and Ha, T. (2009) Cytosolic viral sensor RIG-I is a 5'-triphosphate-dependent translocase on double-stranded RNA. *Science* 323, 1070–1074.

(7) Kawai, T., Takahashi, K., Sato, S., Coban, C., Kumar, H., Kato, H., Ishii, K. J., Takeuchi, O., and Akira, S. (2005) IPS-1, an adaptor triggering RIG-I- and Mda5-mediated type I interferon induction. *Nat. Immunol.* 6, 981–988.

(8) Hou, F., Sun, L., Zheng, H., Skaug, B., Jiang, Q. X., and Chen, Z. J. (2011) MAVS forms functional prion-like aggregates to activate and propagate antiviral innate immune response. *Cell* 146, 448–461.

(9) Basler, C. F., and Garcia-Sastre, A. (2002) Viruses and the type I interferon antiviral system: induction and evasion. *Int. Rev. Immunol.* 21, 305–337.

(10) Randall, R. E., and Goodbourn, S. (2008) Interferons and viruses: an interplay between induction, signalling, antiviral responses and virus countermeasures. *J. Gen. Virol.* 89, 1–47.

(11) Parks, G. D., and Alexander-Miller, M. A. (2013) Paramyxovirus activation and inhibition of innate immune responses. *J. Mol. Biol.* 425, 4872–4892.

(12) Collins, P. L., and Crowe, J. E. (2007) Respiratory syncytial virus and metapneumovirus. In *Fields Virology* (Knipe, D. M., and Howley, P. M., Eds.) pp 1601–1646, Lippincott Williams & Wilkins, Philadelphia.

(13) Spann, K. M., Tran, K. C., Chi, B., Rabin, R. L., and Collins, P. L. (2004) Suppression of the induction of alpha, beta, and lambda interferons by the NS1 and NS2 proteins of human respiratory syncytial virus in human epithelial cells and macrophages [corrected]. *J. Virol.* 78, 4363–4369.

(14) Spann, K. M., Tran, K. C., and Collins, P. L. (2005) Effects of nonstructural proteins NS1 and NS2 of human respiratory syncytial virus on interferon regulatory factor 3, NF-kappaB, and proinflammatory cytokines. *J. Virol.* 79, 5353–5362.

- (15) Lo, M. S., Brazas, R. M., and Holtzman, M. J. (2005) Respiratory syncytial virus nonstructural proteins NS1 and NS2 mediate inhibition of Stat2 expression and alpha/beta interferon responsiveness. *J. Virol* 79, 9315–9319.
- (16) Bossert, B., and Conzelmann, K. K. (2002) Respiratory syncytial virus (RSV) nonstructural (NS) proteins as host range determinants: a chimeric bovine RSV with NS genes from human RSV is attenuated in interferon-competent bovine cells. *J. Virol* 76, 4287–4293.
- (17) Ramaswamy, M., Shi, L., Varga, S. M., Barik, S., Behlke, M. A., and Look, D. C. (2006) Respiratory syncytial virus nonstructural protein 2 specifically inhibits type I interferon signal transduction. *Virology* 344, 328–339.
- (18) Gotoh, B., Komatsu, T., Takeuchi, K., and Yokoo, J. (2001) Paramyxovirus accessory proteins as interferon antagonists. *Microbiol. Immunol.* 45, 787–800.
- (19) Swedan, S., Musiyenko, A., and Barik, S. (2009) Respiratory syncytial virus nonstructural proteins decrease levels of multiple members of the cellular interferon pathways. *J. Virol* 83, 9682–9693.
- (20) Swedan, S., Andrews, J., Majumdar, T., Musiyenko, A., and Barik, S. (2011) Multiple functional domains and complexes of the two nonstructural proteins of human respiratory syncytial virus contribute to interferon suppression and cellular location. *J. Virol* 85, 10090–10100.
- (21) Wu, W., Tran, K. C., Teng, M. N., Heesom, K. J., Matthews, D. A., Barr, J. N., and Hiscox, J. A. (2012) The interactome of the human respiratory syncytial virus NS1 protein highlights multiple effects on host cell biology. *J. Virol* 86, 7777–7789.
- (22) Hastie, M. L., Headlam, M. J., Patel, N. B., Bukreyev, A. A., Buchholz, U. J., Dave, K. A., Norris, E. L., Wright, C. L., Spann, K. M., Collins, P. L., and Gorman, J. J. (2012) The human respiratory syncytial virus nonstructural protein 1 regulates type I and type II interferon pathways. *Mol. Cell. Proteomics* 11, 108–127.
- (23) Ling, Z., Tran, K. C., and Teng, M. N. (2009) Human respiratory syncytial virus nonstructural protein NS2 antagonizes the activation of beta interferon transcription by interacting with RIG-I. *J. Virol* 83, 3734–3742.
- (24) Boyapalle, S., Wong, T., Garay, J., Teng, M., San Juan-Vergara, H., and Mohapatra, S. (2012) Respiratory syncytial virus NS1 protein colocalizes with mitochondrial antiviral signaling protein MAVS following infection. *PLoS One* 7, e29386.
- (25) Elliott, J., Lynch, O. T., Suessmuth, Y., Qian, P., Boyd, C. R., Burrows, J. F., Buick, R., Stevenson, N. J., Touzelet, O., Gadina, M., Power, U. F., and Johnston, J. A. (2007) Respiratory syncytial virus NS1 protein degrades STAT2 by using the Elongin-Cullin E3 ligase. *J. Virol* 81, 3428–3436.
- (26) Atreya, P. L., Peeples, M. E., and Collins, P. L. (1998) The NS1 protein of human respiratory syncytial virus is a potent inhibitor of minigenome transcription and RNA replication. *J. Virol* 72, 1452–1461.
- (27) Ling, Z., Tran, K. C., Arnold, J. J., and Teng, M. N. (2008) Purification and characterization of recombinant human respiratory syncytial virus nonstructural protein NS1. *Protein Expression Purif.* 57, 261–270.
- (28) Pretel, E., Camporeale, G., and de Prat-Gay, G. (2013) The non-structural NS1 protein unique to respiratory syncytial virus: a two-state folding monomer in quasi-equilibrium with a stable spherical oligomer. *PLoS One* 8, e74338.
- (29) Goswami, R., Majumdar, T., Dhar, J., Chattopadhyay, S., Bandyopadhyay, S. K., Verbovetskaya, V., Sen, G. C., and Barik, S. (2013) Viral degradasome hijacks mitochondria to suppress innate immunity. *Cell Res.* 23, 1025–1042.
- (30) Buchner, J., and Kiefhaber, T. (2005) *Protein folding handbook*, Vol. 3, pp 379–410, Wiley-VCH, Weinheim, Germany.
- (31) Myers, J. K., Pace, C. N., and Scholtz, J. M. (1995) Denaturant m values and heat capacity changes: relation to changes in accessible surface areas of protein unfolding. *Protein Sci.* 4, 2138–2148.
- (32) Sanchez, I. E., and Kiefhaber, T. (2003) Evidence for sequential barriers and obligatory intermediates in apparent two-state protein folding. *J. Mol. Biol.* 325, 367–376.
- (33) Zlotnick, A., Johnson, J. M., Wingfield, P. W., Stahl, S. J., and Endres, D. (1999) A theoretical model successfully identifies features of hepatitis B virus capsid assembly. *Biochemistry* 38, 14644–14652.
- (34) Chemes, L. B., Noval, M. G., Sanchez, I. E., and de Prat-Gay, G. (2013) Folding of a cyclin box: linking multitarget binding to marginal stability, oligomerization, and aggregation of the retinoblastoma tumor suppressor AB pocket domain. *J. Biol. Chem.* 288, 18923–18938.
- (35) Tsytlonok, M., and Itzhaki, L. S. (2013) The how's and why's of protein folding intermediates. *Arch. Biochem. Biophys.* 531, 14–23.
- (36) Reimer, U., Scherer, G., Drewello, M., Kruber, S., Schutkowski, M., and Fischer, G. (1998) Side-chain effects on peptidyl-prolyl cis/trans isomerisation. *J. Mol. Biol.* 279, 449–460.
- (37) Brandts, J. F., Halvorson, H. R., and Brennan, M. (1975) Consideration of the Possibility that the slow step in protein denaturation reactions is due to cis-trans isomerism of proline residues. *Biochemistry* 14, 4953–4963.
- (38) Kiefhaber, T., Quaas, R., Hahn, U., and Schmid, F. X. (1990) Folding of ribonuclease T1. I. Existence of multiple unfolded states created by proline isomerization. *Biochemistry* 29, 3053–3061.
- (39) Kiefhaber, T., and Schmid, F. X. (1992) Kinetic coupling between protein folding and prolyl isomerization. II. Folding of ribonuclease A and ribonuclease T1. *J. Mol. Biol.* 224, 231–240.
- (40) Smal, C., Alonso, L. G., Wetzler, D. E., Heer, A., and de Prat Gay, G. (2012) Ordered self-assembly mechanism of a spherical oncoprotein oligomer triggered by zinc removal and stabilized by an intrinsically disordered domain. *PLoS One* 7, e36457.